Harnessing Hydromagnetic Tangent Hyperbolic Hybrid Nanofluids for Enhanced Heat Transfer and Energy Efficiency in Concentrated Solar Power Systems

Abstract

Abstract

In recent years, the development of advanced heat transfer fluids for high-performance thermal systems has attracted significant attention due to increasing energy demands in process industries, electronics cooling, and renewable energy applications. Nanofluids have been widely utilized to enhance thermal efficiency in engineering systems such as concentrated solar power (CSP) technologies. In this study, the energy enhancement, entropy generation, and thermal transport characteristics of an electromagnetic tangent hyperbolic hybrid nanofluid flow in a nonlinear radiative CSP system are investigated.A composite SiO_2–$TiO_2/C_2H_6O_2$ nanofluid flowing over a Riga surface with convective boundary conditions is considered. The transformed governing momentum and energy equations, incorporating the quadratic Boussinesq approximation, hyperbolic tangent rheological model, viscous dissipation, electromagnetic effects, and nonlinear thermal radiation, are derived using similarity transformations. The resulting system is solved numerically using a Chebyshev spectral method coupled with a collocation integration scheme. The results indicate that the thermal profile increases with rising thermal radiation, viscous dissipation, and temperature ratio parameters. Furthermore, entropy generation significantly increases with higher values of the temperature ratio parameter and Weissenberg number, indicating enhanced irreversibility in the system. Also, The velocity slip parameters exhibit dual patterns on the flow mechanism, at the wall ($\eta = 0$) enhances the velocity magnitude, whereas slip away from the wall ($\eta = 1$) lowers the velocity distribution. The findings demonstrate that electromagnetic hybrid nanofluids, when properly optimized, can significantly improve energy efficiency and thermal performance in nonlinear radiative CSP systems.

Keywords: Riga plate; Nonlinear radiation; Composite nanofluid; Tangent hyperbolic fluid; Energy maximization

1 Introduction

Effective thermal management remains a significant issue in engineering modern systems, particularly in high-performance heat exchangers, electrical cooling systems, and renewable energy applications such as concentrated solar power (CSP) [1,2]. The heat transfer strength of traditional fluids (e.g., ethylene glycol and water) is relatively limited by low heat conductivities and weak thermal transport performance, which confines the thermal system's efficiency operation

under high heat flux conditions, Kalsi et al. [3]. To overcome these challenges, nanoparticle suspensions in base solvents were introduced, owing to their improved convective thermal propagation capabilities and higher thermal properties. For decades, studies on nanofluids have increased meaningfully, depicting enhanced heat transfer performance in different industrial applications, Jafari and Wits [4]. Meanwhile, the issues of thermal stability and particle aggregation have restricted the practical deployment of unitary nanoparticles. Thus, hybridized nanofluids have become a promising working fluid class for enhanced thermophysical properties beyond what suspended mono-nanoparticles can achieve, Murugan et al. [5]. Hybrid nanofluids compose a blend of two or more distinct nanoparticle types in base solvents, which influences the synergistic impacts, often leading to better flexibility to thermal gradients, improved stability, and high thermal conductivity compared to unitary nanofluids [6-8]. Experimental studies by Hassaan [9] further establish the capability of hybridized nanofluids in tube-and-shell heat exchangers, demonstrating measurable proficiency enhancements over single nanofluids. Amr and Hassaan [10] presented an experimental study on the multi-wall carbon nanotubes-based application on H_2O nanofluid for a plate thermal exchanger. An improvement in the heat conduction and distribution was reported arising from the thermophysical properties of the fluid.

The various observations on hybrid nanofluids have prompted further investigations on the heat transport and entropy characteristics across different geometries and boundary conditions. While encouraging thermal conductivity is essential, a complete evaluation of thermal systems also necessitates an insight into entropy generation, which measures irreversibilities due to electromagnetic, fluid friction, and heat transfer effects, Nandi et al. [11]. Entropy generation analysis offers an understanding of energy degradation and can guide thermal systems optimization for maximal energy operation, Yusuf et al. [12]. Investigations of flowing hybrid nanofluids have combined the thermodynamic second-law perspective, showing that terms such as magnetic fields, viscous dissipation, and Joule heating significantly affect entropy generation and overall system efficiency, Ekiciler [13]. The interaction of electromagnetic and hybrid nanofluid control strategies, especially Riga plates, has been progressively explored due to their capability to manage thermal fields and flow structure, Adebisi et al. [14]. The Riga plate, an electromagnetic actuator containing alternating magnets and electrodes that produce Lorentz forces, has been broadly discussed as an active flow control mechanism, boundary layers stabilizer, and flow of MHD convective transport enhancement, Mkhatshwa [15]. Recent studies by [16, 17] on nanofluid flows with electromagnetic actuators have demonstrated improved heat transfer and adapted entropy characteristics, emphasizing their potential for innovative thermal management. However, the strength and usefulness of combined electromagnetic actuator and hybrid nanofluid for concentrated solar power can be enhanced when considered with non-Newtonian fluids.

Furthermore, evolving research examines hybrid nanofluids with non-Newtonian fluids, such as tangent hyperbolic fluid in magneto-convective environments and thermal nonlinear radiation effect. Comprehensive analyses of electromagnetically enhanced tangent hyperbolic fluid flow mixtures with nanoparticles find potential usages for combined thermofluid and electromagnetic strategies to boost heat transport performance, Rafique et al. [18]. A tangent hyperbolic fluid is effectively used in modeling shear-thinning characteristics experienced in industrial suspensions, biological fluids, and polymeric solutions. Fatunmbi et al.[19] and Adigun et al. [20] investigated non-Newtonian tangent hyperbolic fluid flows with thermal and external effects over stretching or vertical surfaces. The later focused on magnetohydrodynamic mixed

convection with chemical reaction over a nonlinear stretchable surface, analyzing velocity, temperature, and concentration profiles, whereas the later examined quadratic mixed convection with nonlinear thermal radiation past a vertical elongated sheet, using the Spectral Local Linearization Method to study flow and heat transfer characteristics. Both works highlighted the influence of key parameters on engineering quantities like skin friction, Nusselt, and Sherwood numbers, providing insights for advanced heat transfer and industrial applications. Asogwa et al. [21] and Nadeem et al. [22] examined nanofluid tangent hyperbolic flows with thermal and magnetic effects, reporting high momentum and temperature fields sensitivity to rheological terms. These investigations show the importance of non-Newtonian modeling in heat transfer advanced applications. In renewable energy systems, many analyzes have presented nano and hybrid nanofluids for thermal solar augmentation. Salawu et al. [23] discussed hybridized electromagnetic nanofluids for solar collector maximization, showing a noteworthy improvement in thermal effectiveness. Jamshed et al. [24] studied hybrid tangent hyperbolic nanofluids in thermal solar applications and highlighted their potential for optimization thermal expansion with radiative influences.

Despite these advancements, limited studies have considered the impact of tangent hyperbolic rheology, hybrid nanoparticles, electromagnetic actuation, and nonlinear thermal radiation in CSP systems. Rafique et al. [18] emphasized the essentiality of entropy reduction in magnetically and electrically driven nanofluid flows without considering Riga plate actuation or CSP configurations. Recently, Thumma et al. [17] used spectral and semi-analytical methods to investigate electromagnetic effects in hybrid nanofluid flows; meanwhile, energy maximization and nonlinear radiation in CSP systems remain ignored. Thus, a rich research gap occurs in the study of tangent hyperbolic electromagnetic hybrid nanofluid flow with nonlinear radiative and entropy generation in CSP systems. Filling gaps is vital for enhancing modern solar power sustainability technologies and progressing thermal energy-efficient management strategies. These motivations inspire the current study's focus on combining nonlinear radiative, electromagnetic actuation effects, and dynamics of hybrid nanoparticles for CSP and other energy-intensive geometries.

2 Mathematical formulation description

Consider the momentum and thermal characteristics of a composite SiO_2–$TiO_2/C_2H_6O_2$ tangent hyperbolic hybrid nanofluid flowing over a fixed concentrated Riga plate under nonlinear solar radiation for optimized thermal energy extraction. The dispersed hybrid nanoparticles within the non-Newtonian fluid, combined with ethylene glycol, interact with electromagnetic actuation, viscous heating, gravity, and convective transport, producing a highly controlled flow and heat distribution. The Riga plate-induced Lorentz force ensures stable, continuous convection even at negligible Reynolds numbers and in the absence of magnetic induction. Nanoparticle agglomeration is minimized, preserving surface activity, fluid stability, and thermo-physical enhancements, thereby maximizing **heat transfer performance and energy efficiency, which is critical for the operation of **concentrated solar power systems.

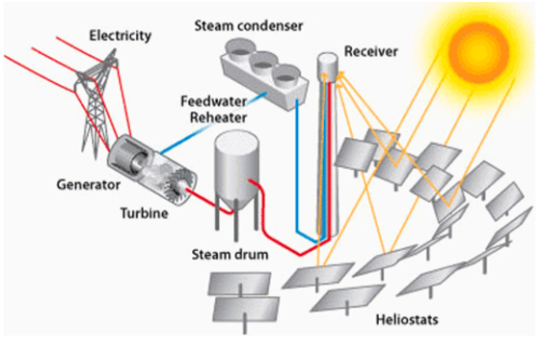

Figure 1: Schematic diagram of CSP

The hyperbolic tangent fluid Cauchy dynamical tensor is considered as presented by [21,23]

$$\bar{\tau} = [tanh(\varphi\bar{\alpha})^r(\mu_0 + \mu_\infty) + \mu_\infty)]\bar{\alpha}, \tag{1}$$

where $\bar{\tau}$ describes the tensor stress, r is the power-law exponent, μ_0 denotes zero viscosity shear rate, μ_∞ presents the infinity viscosity shear rate, and $\bar{\alpha}$ defines the material constant, which is given as:

$$\bar{\alpha} = \left(\frac{1}{2}\sum_i\sum_J \bar{\alpha_{ji}}\bar{\alpha_{ij}}\right)^{1/2} = \left(\frac{1}{2}\prod\right)^{1/2}. \tag{2}$$

While, $\prod = \frac{1}{2}tr[(\nabla F)^T + \nabla F]^2$. When ever $\mu_\infty = 0$, a low viscosity is obtained at infinity and when ever $\varphi\bar{\alpha} < 1$, a shear thin is experienced. As such, equation (1) becomes

$$\bar{\tau} = \bar{\alpha}[\varphi\bar{\alpha}^r]\mu_0 = \bar{\alpha}[(1 + \varphi\bar{\alpha} - 1)^r]\mu_0 \approx \bar{\alpha}[(m(\varphi\bar{\alpha} - 1) + 1)]\mu_0. \tag{3}$$

With the tangent hyperbolic material consumption is considered negligible, and the flow medium wall is exposed to continuous Biot-type convective cooling to keep the system from excessive heat and possible explosion. Therefore, energy and mass are conserved. Taking from the highlighted assumptions, the thermodynamic model for the nonlinear thermal radiative hybridized tangent hyperbolic nanofluid flow with viscous heating, electromagnetic actuator, and thermal convection is considered as in [25-27]

$$\frac{d\psi}{dy} = 0, \qquad \Rightarrow \psi = \psi_0 \tag{4}$$

$$\rho_{hf}\psi_0\frac{d\psi}{dy} = -\frac{dP}{dx} + \mu_{hf}\left[\frac{d^2\psi}{dy^2}\left\{1 - r\left(1 - \varphi\frac{d\psi}{dy}\right)\right\}\right] + \frac{\pi J_0 M_0}{8}\exp\left(-\frac{\pi}{b}y\right) + \rho_{hf}g\left\{\alpha_1(\phi - \phi_s) + \alpha_2(\phi - \phi_s)^2\right\}, \tag{5}$$

$$(\rho C_p)_{hf}\psi_0\frac{d\phi}{dy} = k_{hf}\frac{d^2\phi}{dy^2} + \mu_{hf}\left(\frac{d\psi}{dy}\right)^2\left[(1 - r) + r\varphi\left(\frac{d\psi}{dy}\right)\right] + \frac{16\sigma}{3\kappa}\left(3\phi^2\left(\frac{d\phi}{dy}\right)^2 + \phi^3\frac{d^2\phi}{dy^2}\right) + Q_0(\phi - \phi_s), \tag{6}$$

the suitable boundary constraints are considered following, Hassan et al. [24]:

$$\begin{aligned} \psi - \gamma_1 \frac{d\psi}{dy}\left((1-r) + r\varphi\frac{d\psi}{dy}\right) = 0, \qquad k_{hf}\frac{d\phi}{dy} = \epsilon_1(-\phi_c + \phi) \qquad \text{at} \quad y = 0, \\ \psi + \gamma_2 \frac{d\psi}{dy}\left((1-r) + r\varphi\frac{d\psi}{dy}\right) = 0, \qquad k_{hf}\frac{d\phi}{dy} = \epsilon_2(\phi - \phi_s) \qquad \text{at} \quad y = h. \end{aligned} \tag{7}$$

where ψ is the velocity component in y direction, μ_{hf} represents hybrid nanofluid viscosity, P denotes pressure, ρ_{hf} is the hybrid nanofluid density, g is gravity, φ defines the hyperbolic tangent parameter, ϕ is fluid temperature, C_p presents thermal capacity, k_{hf} defines hybrid nanofluid heat conductivity, b is the breadth of the electrode and magnet, M_0 is the magnetized of magnetic, J_0 represents the current density, and α_1 and α_2 are the heat expansivity coefficients separately. Also, the terms σ presents the Stefan-Boltzmann constant, ϵ_1 and ϵ_2 give the boundary thermal surface coefficients, κ is the heat absorption, γ_1 and γ_2 connote boundary velocity slip coefficients, Q_0 presents heat generation, and ϕ_c and ϕ_s describe the device surface temperature respectively.

The composite nanofluid is synthesized by the hybridization of SiO_2 nanoparticle in $C_2H_6O_2$ fluid with volume fraction (ξ_1) efficient and TiO_2 nanoparticle dispersed on it with volume fraction (ξ_2) concentration, as demonstrated in Table 1.

Table 1: Thermophysical quantities of the nanofluids

Quantities	Nanofluid properties
Fluid viscosity	$\mu_{nf} = (1-\xi)^{-5/2}\mu_f$
Fluid density	$\rho_{nf} = (1-\xi)\rho_f - \xi\rho_s$
Heat capacity	$(\rho C_p)_{nf} = (\rho C_p)_f(1-\xi) - \xi(\rho C_p)_s$
Heat conductivity	$\frac{k_{nf}}{k_f} = \frac{2\xi(k_s-k_f)+(2k_f+k_s)}{\xi(k_f-k_s)+(2k_f+k_s)}$
Heat expansivity	$(\rho\alpha)_{nf} = \left(\xi\frac{(\rho\alpha)_s}{(\rho\alpha)_f} + 1 - \xi\right)(\rho\alpha)_f$

The thermophysical quantities of the nanofluid are given in Table 1, following [28, 29], and the density of fluid and solid are ρ_f and ρ_s, ξ denotes the volume fraction of the nanoparticle. The particles heat conductivity of fluid and solid are k_f and k_s, the thermal capacity of fluid and solid are $(C_p)_f$ and $(C_p)_s$, and μ_f fluid viscosity.

Table 2: Thermophysical quantities of the composite nanofluid

Quantities	Properties of the hybrid nanofluid
Viscosity	$\mu_{hf} = (1-\xi_1)^{-5/2}(1-\xi_2)^{-5/2}\mu_f$
Density	$\rho_{hf} = [(1-\xi_1)\{(1-\xi_2)\rho_f + \xi_1\rho_{o1}\}] + \xi_2\rho_{o2}$
Thermal conduction	$\frac{k_{hf}}{k_{af}} = \frac{(k_{o2}+2k_{af})-2\xi_1(k_{af}-k_{o2})}{(k_{o2}+2k_{af})-\xi_1(k_{o2}-k_{af})}, \frac{k_{af}}{k_f} = \frac{k_{o1}+(2k_f)-2\xi_2(k_{af}-k_{o2})}{(k_{o1}+2k_f)-\xi_2(k_{o1}-k_f)}$
Thermal capacity	$(\rho C_p)_{hf} = [(1-\xi_1)\{(\rho C_p)_f(1-\xi_2) + (\rho C_p)_{o1}\xi_2\}] + (\rho C_p)_{o2}\xi_1$
Thermal expansivity	$(\rho\alpha)_{hf}$=$(\rho\alpha)_f(1-\xi)\left(\xi_1\frac{(\rho\alpha)_{o1}}{(\rho\alpha)_f} + 1 - \xi_1\right) + \xi_2(\rho\alpha)_{o2}$

Table 2 presents the hybrid nanofluid thermophysical terms, following [28, 29]. The terms k_{hf}, ρ_{hf}, $(\rho C_p)_{hf}$, μ_{hf}, and α_{hf} define the hybrid nanofluid thermal conductivity, density, thermal capacity, viscosity, and thermal expansivity separately. The nanosolid concentrated particle for the composite nanofluid is $\xi_{hf} = \xi_1 + \xi_2$. A transformed invariant dimensionless equations

together with the boundary conditions are determined through the similarity quantities, as demonstrated by Hassan et al. [24] as:

$$\eta = \frac{y}{a}, \qquad \psi = \frac{\mu}{c\rho} w(\eta), \quad \text{and} \quad \phi = (\phi_c - \phi_s)\, T(\eta) + \phi_s. \tag{8}$$

This resulted in the dimensionless transformation equations, the given variables of equation (8) are employed to have:

$$A_2(1-r)w^{''}(\eta) - A_1 Re w^{'}(\eta) + A_2 r We w^{'}(\eta) w^{''}(\eta) + G + A_3\lambda[T(\eta) + \gamma T^2(\eta)] + Me^{-\omega\eta} = 0, \tag{9}$$

$$\begin{aligned} & A_5 T''(\eta) - A_4 Pr\, Re\, T'(\eta) \\ & + Ra\, Pr\Big[3\big(1 + (\zeta - 1)T^2(\eta)\big)\big(T'(\eta)\big)^2 + \big(1 + (\zeta - 1)T^3(\eta)\big)T''(\eta)\Big] \\ & + Pr\, Q\, T(\eta) + A_2 Pr\, Ec\left\{A_2 \frac{rWe}{2}\big(w'(\eta)\big)^3 + (1-r)\big(w'(\eta)\big)^2\right\} = 0. \end{aligned} \tag{10}$$

with transformed boundary conditions as:

$$\begin{aligned} & w(\eta) - \beta_1 w^{'}(\eta)\left\{(1-r) + \frac{rWe}{2} w^{'}(\eta)\right\} = 0, \quad T^{'}(\eta) - A_5\delta_1[T(\eta) - 1] = 0 \ \text{ at } \ \eta = 0, \\ & w(\eta) + \beta_2 w^{'}(\eta)\left\{(1-r) + \frac{rWe}{2} w^{'}(\eta)\right\} = 0, \quad T^{'}(\eta) + A_5\delta_2 T(\eta) = 0 \quad \text{at } \ \eta = 1. \end{aligned} \tag{11}$$

The embedded terms are individual defines as the: $Re = \frac{a\rho_f\psi_0}{\mu_f}$ Reynolds number, $We = \frac{2\varphi\mu_f}{a^2\rho_f}$ Weissenberg number, $G = -\frac{a^3\rho_f}{\mu_f}\frac{dP}{dx}$ pressure gradient, $\lambda = \frac{ga^3\alpha_1(\phi_c - \phi_s)\rho_f}{\mu_f^2}$ thermal convection, $\gamma = \frac{\alpha_2(\phi_c - \phi_s)}{\alpha_1}$ nonlinear convection, $M = \frac{a^2\pi J_0 M_0}{8\rho_f\psi_0}$ magnetic term, $\omega = \frac{a\pi}{b}$ magnetized magnetic, $Pr = \frac{\mu_f C_p}{k_f}$ Prandtl number, $Ec = \frac{\mu_f^2}{\rho_f^2 a^2 C_p(\phi_c - \phi_s)}$ Eckert number, $Ra = \frac{16\varsigma\phi_s^3}{3\kappa k_f}$ radiation, $\beta_i = \frac{\gamma_i}{a}(i = 1, 2)$ is velocity slip, $\delta_i = \frac{a\epsilon_i}{k}(i = 1, 2)$ wall convective cooling, and $\zeta = \frac{T_s}{T_c}$ thermal ratio. Table 3 gives the nanoparticles thermal properties and the base-fluid. The nanofluid terms A_1, A_2, A_3, A_4, and A_5 with the respective thermophysical quantities:

$$\begin{aligned} & A_1 = (1-\xi_2)\left[\xi_1\frac{\rho_{o1}}{\rho_f} + (1-\xi_1)\right] + \xi_2\frac{\rho_{o2}}{\rho_f}, \ A_3 = (1-\xi_2)\left[(1-\xi_1) + \xi_1\frac{\alpha_{o1}}{\alpha_f}\right] + \xi_2\frac{\alpha_{o2}}{\alpha_f}, \\ & A_2 = (1-\xi_1)^{-5/2}(1-\xi_2)^{-5/2}, \ A_4 = (1-\xi_1)\left\{(1-\xi_2) + \xi_2\frac{(\rho C_p)_{o1}}{(\rho C_p)_f}\right\} + \xi_1\frac{(\rho C_p)_{o2}}{(\rho C_p)_f}, \\ & A_5 = \frac{(k_{o2} + 2k_{af}) - 2\xi_2(k_{af} - k_{o2})}{(k_{o2} + 2k_{af}) - \xi_2(k_{o2} - k_{af})}, \frac{k_{af}}{k_f} = \frac{(k_{o1} + 2k_f) - 2\xi_1(k_f - k_{o1})}{(k_{o1} + 2k_f) - \xi_1(k_{o1} - k_f)}. \end{aligned} \tag{12}$$

Table 3: The nanoparticles thermal properties and the base-fluid

Properties	$\alpha(1/K)$	$\rho(kg/m^3)$	$k(W/mK)$	$C_p(J/kgK)$
$C_2H_6O_2$	5.70	1110	0.253	22,000
SiO_2	1.67	2650	1.5	730
TiO_2	0.9×10^{-5}	4250	8.953	686

2.1 Entropy Generation Formulation

With electromagnetic actuator, the second law of thermodynamic is used to determine the hybrid tangent hyperbolic nanofluid heat irreversibility, as given by [32, 33]. This assists keeping the thermal system dynamical equilibrium. Thus, the entropy generation formulation in dimensional form as:

$$E_g = \frac{k_{hf}}{\phi_s^2}\left(\frac{d\phi}{dy}\right)^2 + \frac{16\sigma}{3\kappa}\left(3\phi^2\left(\frac{d\phi}{dy}\right)^2 + \phi^3\frac{d^2\phi}{dy^2}\right) + \frac{1}{\phi_s}\left[\mu_{hf}\left(\frac{d\psi}{dy^2}\right)^2\left\{1 - r\left(1 - \varphi\frac{d\psi}{dy}\right)\right\}\right]. \tag{13}$$

Utilizing the terms defined in equation (8) on the equation (13), resulting in a entropy generation dimensionless equation as:

$$\begin{aligned} E_m = \frac{E_g}{\xi} = A_5\left(T^{'}(\eta)\right)^2 + PrEc\left\{A_2\frac{rWe}{2}(w^{'}(\eta))^3 + A_2(1-r)(w^{'}(\eta))^2\right\} + \\ A_5 Ra\left(3(1+(\zeta-1)T(\eta)^2(\zeta-1)(T^{'}(\eta))^2 + (1+(\zeta-1)T(\eta)^3T^{'}(\eta)\right). \end{aligned} \tag{14}$$

Therefore, equation (14) satisfied the heat transport irreversibility and non-Newtonian viscous heating irreversibility.

2.2 Engineering dynamical wall characteristics

The composite hyperbolic tangent nanofluid engineering dynamical characteristics at the wall are represented as the Skin friction (ψ_f) and thermal gradient (ϕ_h). These wall characteristics are vital in engineering thermal system for the prediction of their various activities. The description of the models mathematically are given as:

$$\psi_f = \frac{\tau_f}{u_f^2\rho_{hf}}, \qquad \phi_h = \frac{xQ_f}{k_{hf}(\phi_c - \phi_s)}, \tag{15}$$

whereas τ_f and Q_f are modelled as:

$$\tau_f = \mu_{hf}\frac{d\psi}{dy}\left((1-r) + r\varphi\frac{d\psi}{dy}\right)\Big|_{y=0}, \qquad Q_f = -k_{hf}\left(\frac{16\sigma\phi^3}{\kappa} + 1\right)\frac{d\phi}{dy}\Big|_{y=0}. \tag{16}$$

Introducing the quantities in (8) into the models (15) and (16), an invariant transformed models are gotten as:

$$w_f Re_x^{0.5} = A_2 w^{'}(0)\left((1-r) + \frac{rWe}{2}w^{'}(0)\right),\ T_h Re_x^{-0.5} = -A_5\left(1 + Ra((\zeta-1)+1)T(0)^3\right)T^{'}(0) \tag{17}$$

3 Semi-Analytical methodology

The coupled boundary value invariant transformed equations (9-11) are solved through a Chebyshev semi-analytical technique combined with an integrating collocation scheme. This methodology is employed due to its consistent, stability, convergence and accuracy. Following Chebaane [32, 33], the solution algorithms are presented.

3.1 Solution procedures

Am assumed solution is considered individually for the momentum function $w(\eta)$ and energy function $T(\eta)$ as the sum of functions in Chebyshev polynomial given as:

$$w(\eta) = \sum_{i=0}^{m} f_i H_i\left(\frac{2\eta}{\varsigma} - 1\right), \quad \text{and} \quad T(\eta) = \sum_{i=0}^{m} g_i H_i\left(\frac{2\eta}{\varsigma} - 1\right), \tag{18}$$

where f_i and g_i are unknown constants that must be determined. The term $H_i\left(\frac{2\eta}{\varsigma} - 1\right)$ represents the basis shifted Chebyshev function in $[-1, 1]$ to $[0, \varsigma]$, and ς presents the boundary far domain. To evaluate the values of the unknown constant, the defined basis Chebyshev functions of (18) are introduced to the transformed boundary conditions (11) to become:

$$\left\{\sum_{i=0}^{m} f_i H_i\left(\frac{2\eta}{\varsigma} - 1\right) - \beta_1 \frac{d}{d\eta}\left(\sum_{i=0}^{m} f_i H_i\left(\frac{2\eta}{\varsigma} - 1\right)\right)\left[1 + \frac{We}{2}\frac{d}{d\eta}\left(\sum_{i=0}^{m} f_i H_i\left(\frac{2\eta}{\varsigma} - 1\right)\right)\right]\right\}_{\eta=0} = 0, \tag{19}$$

$$\left\{\frac{d}{d\eta}\left(\sum_{i=0}^{m} g_i H_i\left(\frac{2\eta}{\varsigma} - 1\right)\right) - A_5\delta_1\left[\sum_{i=0}^{m} g_i H_i\left(\frac{2\eta}{\varsigma} - 1\right) - 1\right]\right\}_{\eta=0} = 0, \tag{20}$$

$$\left\{\sum_{i=0}^{m} f_i H_i\left(\frac{2\eta}{\varsigma} - 1\right) + \beta_2 \frac{d}{d\eta}\left(\sum_{i=0}^{m} f_i H_i\left(\frac{2\eta}{\varsigma} - 1\right)\right)\left[1 + \frac{We}{2}\frac{d}{d\eta}\left(\sum_{i=0}^{m} f_i H_i\left(\frac{2\eta}{\varsigma} - 1\right)\right)\right]\right\}_{\eta=\varsigma} = 0, \tag{21}$$

$$\left\{\frac{d}{d\eta}\left(\sum_{i=0}^{m} g_i H_i\left(\frac{2\eta}{\varsigma} - 1\right)\right) + A_5\delta_2\sum_{i=0}^{m} g_i H_i\left(\frac{2\eta}{\varsigma} - 1\right)\right\}_{\eta=\varsigma} = 0. \tag{22}$$

Then, the residues $R_w(\eta,\ f_i,\ g_i)$, and $R_T(\eta,\ f_i,\ g_i,\ d_i)$ are gotten from the basis Chebyshev functions imposed on the transformed model (9) and (10). Hence, the residue errors are minimized as possible to zero through integrating collocation method defined as:

$$\delta_c(\eta - \eta_j) = \begin{cases} 1, & \eta = \eta_j \\ 0, & \text{otherwise,} \end{cases}$$

$$\int_0^{\varsigma} R_w \delta_c(\eta - \eta_j)\, d\eta = R_w(\eta_j) = 0, \quad \text{for } j = 1,\ 2, .., Z-1 \tag{23}$$

$$\int_0^{\varsigma} R_T \delta_c(\eta - \eta_j)\, d\eta = R_T(\eta_j) = 0, \quad \text{for } j = 1,\ 2, .., Z-1 \tag{24}$$

where $\eta_j = \frac{\varsigma}{2}\left(1 - cos\left(\frac{\pi j}{Z}\right)\right)$ denotes the shifted Gauss-Lobatto nodes. Therefore, $3Z+3$ algebraic system of equations (19-24) is generated with $3Z+3$ unknown constants (f_i and g_i). The solutions to the algebraic system of equations are determined using the Newton method, and the constant values are evaluated. The models are in finite range; such that the value of ς is 1 (i.e. $\varsigma = 1$).

4 Results and description

For further understanding of and effective discussion of results obtained in this study, we have included some graphs to portray the influence of key parameters on the dimensionless velocity and thermal distribution in the system. The included graphs are discussed appropriately under this section.

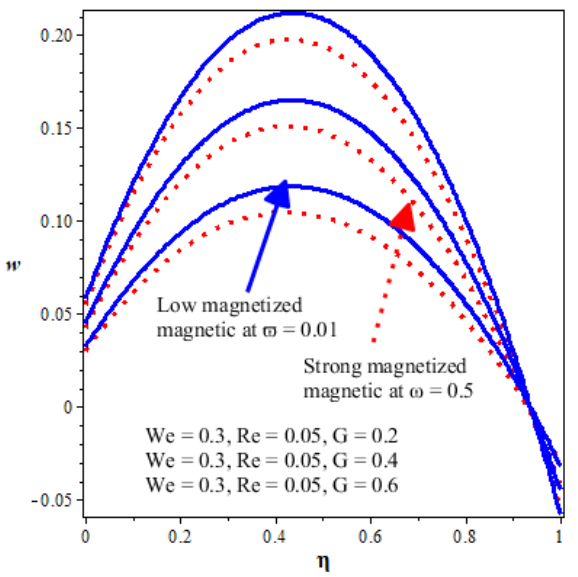

Figure 2: Variational effect of pressure gradient G

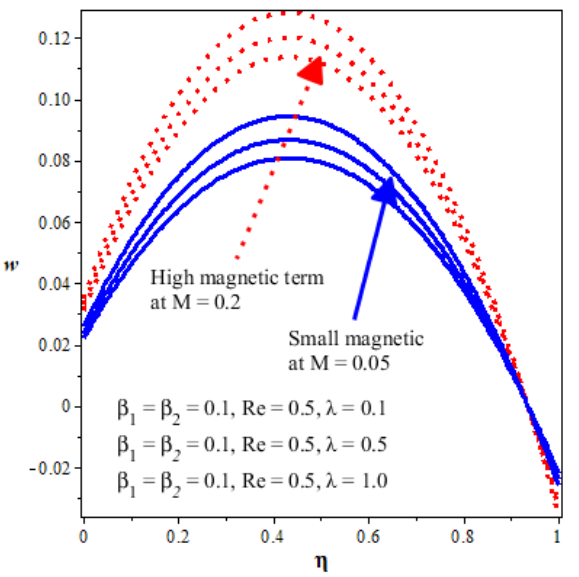

Figure 3: Velocity field for increasing λ

Figure 2 illustrates the velocity profiles $w()$ against η for various values of the pressure gradient parameter G, in the presence of = 0.01 and = 0.1, while keeping We=0.3 and Re=0.05 fixed. It is observed that an increase in G leads to a corresponding enhancement in the velocity distribution for both values of ω. However, the velocity profile is higher at the lower rotation parameter (= 0.01) compared to the higher value = 0.1, indicating that increased rotational effects tend to suppress fluid motion. Furthermore, Figure 3 depicts the influence of the thermal convection parameter λ on the velocity profiles under conditions of high magnetic parameter (M=0.2) and low magnetic parameter (M=0.05). It is evident that the velocity field increases with increasing for both cases of M, due to enhanced buoyancy effects. Additionally, it is observed that the velocity distribution is lower for the smaller magnetic parameter (M=0.05) compared to the higher magnetic parameter (M=0.2), suggesting that stronger magnetic effects promote fluid motion in the present configuration.

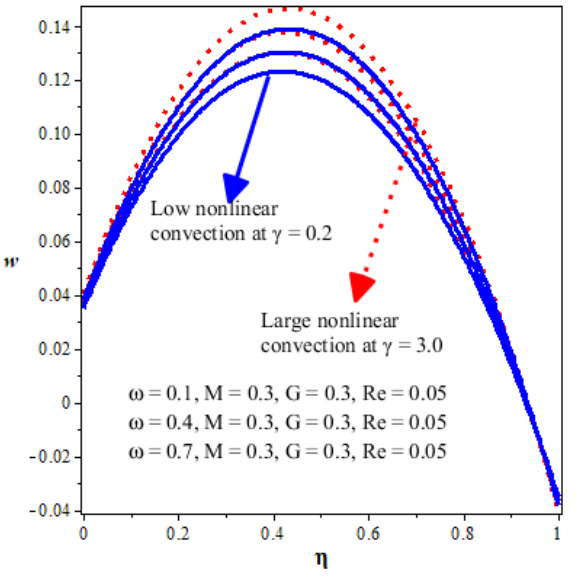

Figure 4: Velocity profile for varying γ

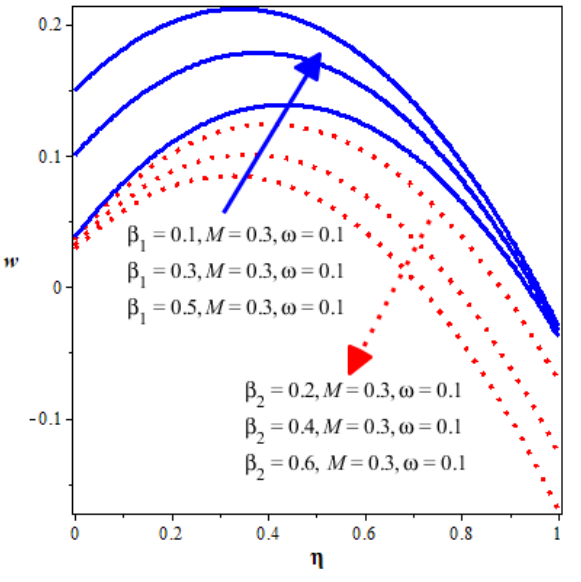

Figure 5: Velocity field for rising β_1&β_2

Figure 4 demonstrates that a rise in ω from 0.1 to 0.7 causes a decline in the velocity distribution for both low nonlinear thermal convection $\gamma = 0.2$ and high nonlinear thermal convection $\gamma = 3.0$. It is noted that the velocity profile is higher for large γ than in the presence of low γ. The graph indicating the variation of β_1 and β_2 on the flow dynamics of the tangent hyperbolic fluid is presented in Figure 5. The picture illustrates the dual character exhibited by the velocity profiles as β_1, β_2 changes values. It is noted that while a rise in β_1 improves the magnitude of the velocity distribution, there is a depletion of the profile due to higher values of β_2

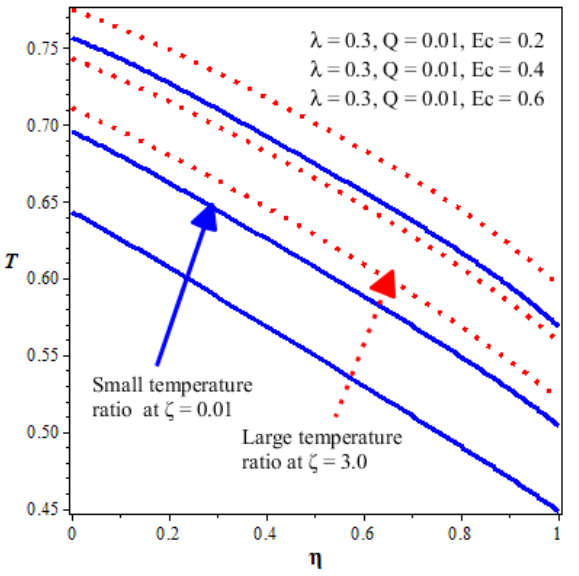

Figure 6: Heat distribution for various Ec

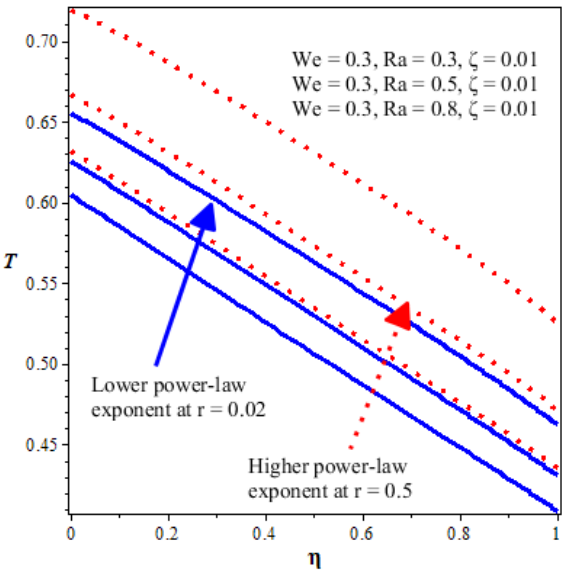

Figure 7: Thermal propagation for rising Ra

Figures 6–9 present the effects of various governing parameters on the thermal distribution within the system. Figure 6 depicts the influence of the Eckert number Ec on the temperature profile in the presence of both low ($\zeta = 0.01$) and higher values of the temperature ratio parameter ζ. It is observed that an increase in Ec leads to a corresponding rise in the temperature

distribution for both cases, owing to enhanced viscous dissipation. Furthermore, the thermal profile becomes more pronounced at higher values of ζ, which is attributed to the thickening of the thermal boundary layer as ζ increases. Similarly, Figure 7 illustrates the effect of the radiation parameter Ra on the temperature distribution. An increase in Ra results in a significant enhancement of the thermal field, indicating that thermal radiation contributes additional heat to the system. This behavior is consistent for both low and high values of the power-law exponent parameter r. Moreover, larger values of r produce a stronger thermal profile compared to smaller values, suggesting increased thermal sensitivity of the fluid. In addition, it is observed that increasing the rotation parameter ω leads to a reduction in the surface temperature, indicating that rotational effects tend to suppress thermal energy within the system. In the same way, the heat profile magnifies as the radiation term Ra increases in magnitude as demonstrated in Figure 7. In the presence of both low and large power-law exponent parameter (r), magnifying the values of Ra causes the thermal bounding surface to enlarge and thus, the surface temperature increases as noted in Figure 7. Moreover, the thermal profile is stronger in the presence of large values of r than that of low values of r. It is noted that higher values of ω decreases the surface temperature as compared to values of ω.

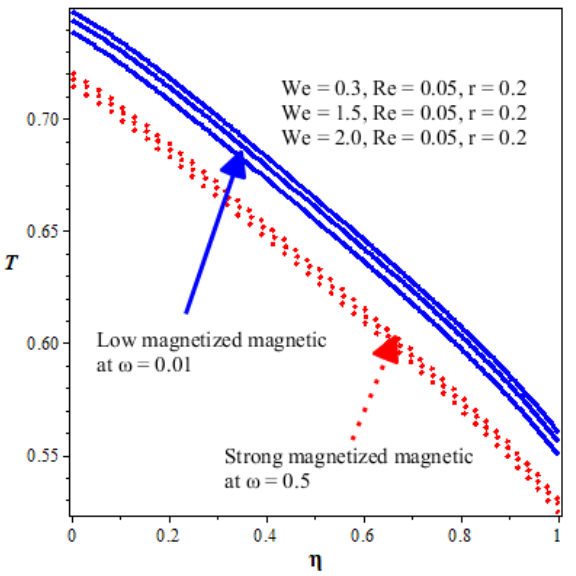

Figure 8: Temperature field for different We

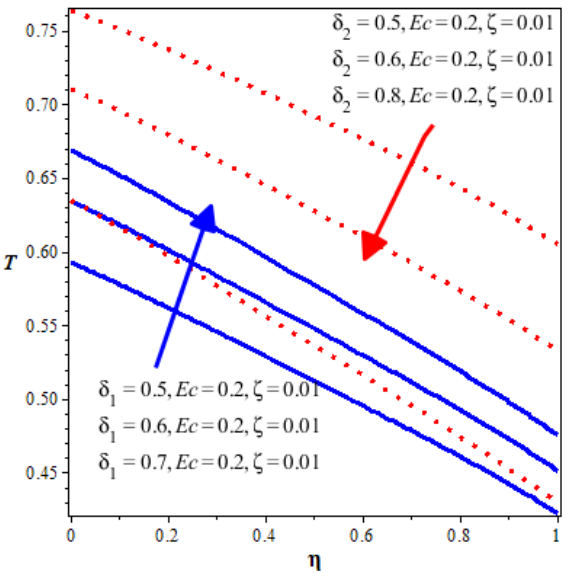

Figure 9: Thermal slip on heat transfer

Figure 8 displays the reaction of the thermal profile versus η as the fluid material parameter (Weissenberg number) We increases in strength. An increase in We magnifies the thermal distribution for large and low values of ω as shown in this figure. The behaviour of the thermal profile for variation in thermal convective cooling is depicted in Figure 9. The thermal convective cooling δ_1 at $\eta = 0$ propels a rise in the temperature distribution, whereas δ_2 which is at $\eta = 1$ causes the thermal profile to deplete as noted in this figure.

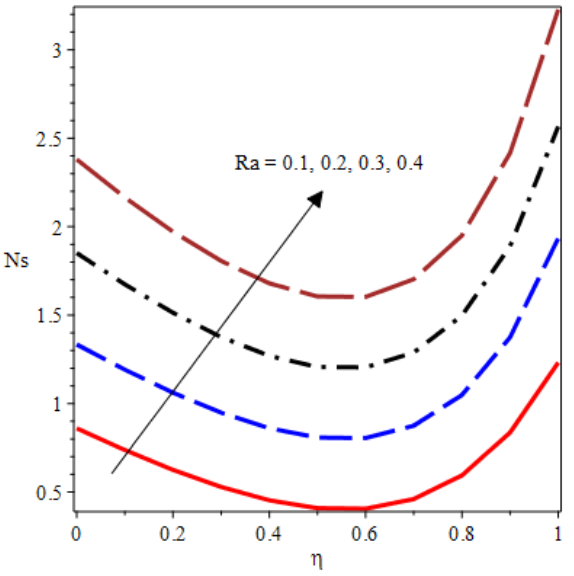

Figure 10: entropy generation for different Ra

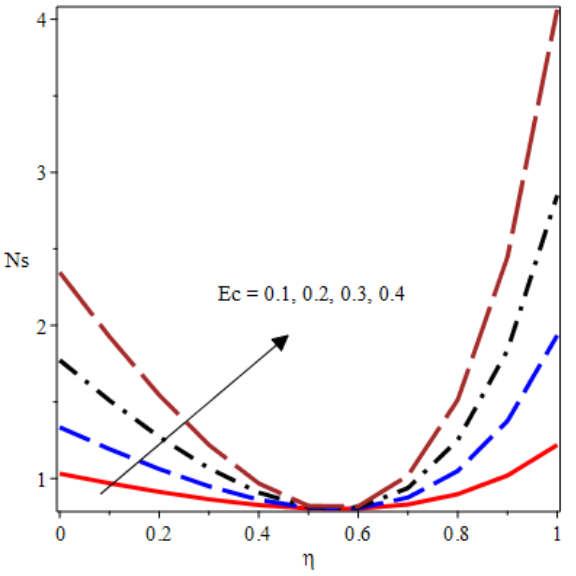

Figure 11: Entropy generation for Ec

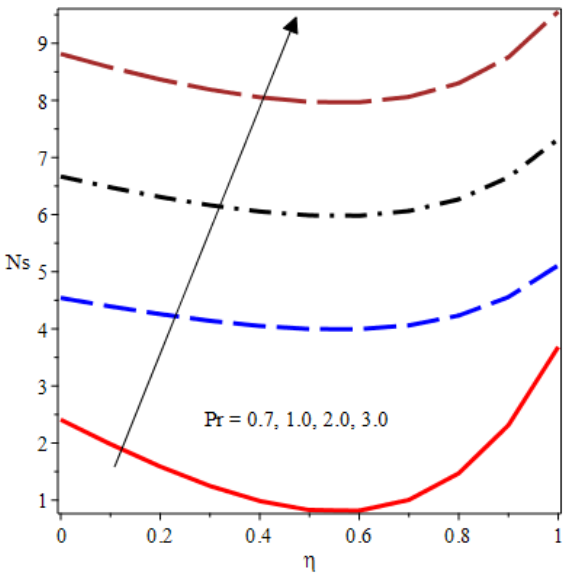

Figure 12: entropy generation for different Pr

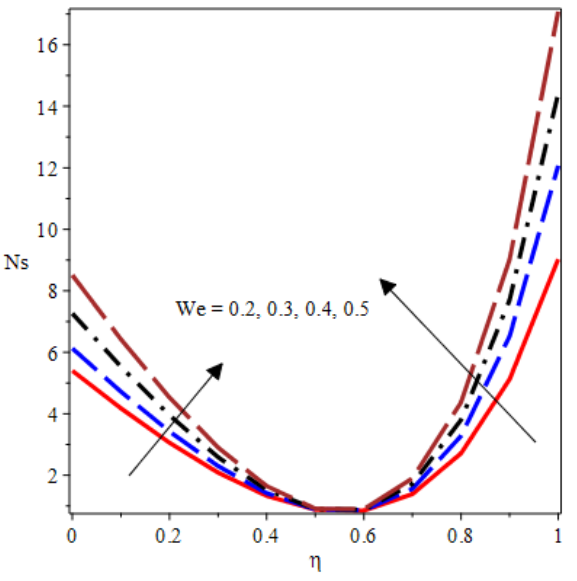

Figure 13: Entropy generation for We

Figures 10-13 portray the behaviour of the entropy generation number profiles for variations in Ra, Ec, Pr and We respectively. The profiles of Ns reveal that there is an increase in the entropy generation for escalating values of Ra, Ec, Pr and We as noted in this pictures. Thus, entropy generation optimization can be achieved by reducing the magnitudes of each of these parameters in the system.

5 Conclusion

This study investigates the energy enhancement, entropy generation, and thermal transport characteristics of an electromagnetic tangent hyperbolic hybrid nanofluid flow in a nonlinear radiative concentrated solar power (CSP) system, employing a composite SiO_2–$TiO_2/C_2H_6O_2$

nanofluid. The transformed governing momentum and energy equations, incorporating the quadratic Boussinesq approximation, hyperbolic tangent rheological model, viscous dissipation, electromagnetic effects, and nonlinear thermal radiation, were formulated using appropriate similarity transformations. The resulting system of equations was solved using a Chebyshev spectral method combined with a collocation integration scheme. The results demonstrate that electromagnetic hybrid nanofluids, when properly optimized, have significant potential for enhancing energy efficiency and thermal performance in nonlinear radiative CSP systems.

The main findings of the study are summarized as follows:

- The velocity profiles increase with rising pressure gradient and nonlinear thermal convection parameters for both low and high values of the magnetic parameter, indicating enhanced fluid motion under stronger driving forces.

- The velocity slip parameters exhibit dual effects on the flow behavior. Slip at the wall ($\eta = 0$) enhances the velocity magnitude, whereas slip away from the wall ($\eta = 1$) reduces the velocity distribution.

- Entropy generation increases with higher values of radiation parameter, Eckert number, Prandtl number, and fluid material parameters. Therefore, minimizing these parameters is essential for achieving optimal system performance and reducing irreversibility.

- The thermal boundary layer thickness increases with increasing linear and nonlinear thermal radiation, Eckert number, and temperature ratio parameter. The thermal profile is more pronounced for larger values of the power-law exponent, while higher magnetic parameter values reduce the surface temperature compared to lower values, indicating a cooling effect of the magnetic field.

References

[1] S. Kalsi, S. Kumar, A. Kumar, T. Alam, A. Sharma, A.S. Yadav, A review on hybrid nanofluids for heat transfer: advancements, synthesis, challenges and applications, Discov Appl Sci., 7 698 (2025) s42452.

[2] S.O. Salawu E.I. Akinola, O.Y. Oludoun, O.M. Ogunlaran, J.A. Akinpelu, Heat radiation absorption and irreversibility of electromagnetic Williamson hybridized Al2O3-CoF e2O4/H2O nanofluid: A concentrated power generation, J. of the Indian Chem. Soc., 101 (2024) 101225.

[3] S. Kalsi, S. Kumar, A. Kumar, T. Alam, D. Dobrotă, Thermophysical properties of nanofluids and their potential applications in heat transfer enhancement: a review, Arab J Chem., 16(11) (2023) 105272.

[4] D. Jafari, W.W. Wits, The utilization of selective laser melting technology on heat transfer devices for thermal energy conversion applications: a review, Renew Sustain Energy Rev., 91 (2018) 420-442.

[5] R.D. Murugan, N. Sivakumar, N. Tarakaramu, H. Ahmad, S. Askar, Entropy generation on MHD motion of hybrid nanofluid with porous medium in presence of thermo-radiation and ohmic viscous dissipation, Discover Appl. Sci., 6 (2024) s42452.

[6] M. Shoaib, M.A.Z. Raja, M.T. Sabir, M. Awais, S. Islam, Z. Shah, P. Kumam, Numerical analysis of 3-D MHD hybrid nanofluid over a rotational disk in presence of thermal radiation with Joule heating and viscous dissipation effects using Lobatto IIIA technique, Alex Eng J., 60(4) (2021) 3605-3619.

[7] F. Wang, E.O. Fatunmbi, A.T. Adeosun, S.O. Salawu, I.L. Animasaun, I.E. Sarris, Comparative analysis between copper ethyleneglycol and copper-iron oxide ethylene-glycol nanoparticles both experiencing Coriolis force, velocity and temperature jump, Case Studies in Thermal Engin., 47 (2023) 103028.

[8] A.M. Rashad, M.A. Nafe, D.A. Eisa, Heat variation on MHD Williamson hybrid nanofluid flow with convective boundary condition and ohmic heating in a porous material, Sci Rep., 13 (2023) 6071.

[9] A.M. Hassaan, Evaluating experimentally the viability of employing hybrid nanofluids as an operating fluid in a shell-and-tube heat exchanger, Sci Rep., 15 (2025) 4030.

[10] M. Amr, Hassaan, An experimental investigation for the use of multi-wall carbon nanotubes based on water nanofluid in a plate heat exchanger, Heat Transf. Res., 53 (16) (2022) 19-34.

[11] S. Nandi, M. Das, B. Kumbhakar, Entropy generation in magneto-Casson nanofluid flow along an inclined stretching sheet under porous medium with activation energy and variable heat source/sink, J Nanofluids, 11(1) (2022) 17-30.

[12] T.A. Yusuf, S.O. Salawu, S.O. Adesanya, J.C. Ukaegbu, Irreversibility analysis in an electro-osmotically driven flow using ternary hybrid nanofluids in a microchannel with a porous material, ZAMM-J. of Appl. Maths., 24 (2024) e202300667.

[13] R. Ekiciler, Performing SiO2-MWCNT/water hybrid nanofluid with differently shaped nanoparticles to enhance first-and second-law features of flow by considering a two-phase approach, J Therm Anal Calorim., 149 (2024) 1725-1744.

[14] O. Adebisi, O.A. Ajala, A.A. Bepo, M. Taiwo, Thermal performance of hybrid nanoparticles on radiative flow with slip boundary condition under the influence of Riga plate, Int. J. Adv. Multidisc. Res. Stud., 5(1) (2025) 1270-1279.

[15] M.P. Mkhatshwa, Entropy production on mixed convection stagnation point flow of non-linear radiative fourth-grade hybrid nanofluid through a stretchable Riga surface, Discov. Appl. Sci. 6 (2024) 234.

[16] A. Buhari, M.N. Sarki, S.A. Bawa, Transient electro-magneto hydrodynamic control of hybrid nanofluid flow over 2D Riga plate: Entropy generation and stability analysis, Int. J. of Sci. for Global Sust., 11 (2025) 1854.

[17] T. Thumma, S.R. Mishra, S.O. Salawu, Spectral Chebyshev technique for heat transfer analysis of hybrid CoF e2O4–MoS2 nanofluid flow with electromagnetic and melting surface effects in slippage wedge, J. of Thermal Analy. and Calor., 34 (2025) s10973.

[18] K. Rafique, Z. Mahmood, Adnan, U. Khan, T. Muhammad, M. A. El-Rahman, S.A. Bajri, H.E. Khalifa, Numerical investigation of entropy generation of Joule heating in non-axisymmetric flow of hybrid nanofluid towards stretching surface, J. of Comput. Design and Engin., 11 (2024) 146-160. E. O. Fatunmbi, F. Mabood, H. Elmonser, I. Tlili. Magneto-hydrodynamic nonlinear mixed convection flow of reactive tangent hyperbolic nano fluid passing a nonlinear stretchable surface. physica scripta 96(1) (2021): 015204.

[19] A. J. Adigun, E. O. Fatunmbi, and C. U. Boneze. Quadratic Mixed Convection Tangent Hyperbolic Stratified Fluid Flow Past a Vertical Elongated Sheet with Nonlinear Thermal Radiation: Spectral Local Linearization Method." International Journal of Mathematical Sciences and Optimization: Theory and Applications 8(2), (2022): 131-148.

[20] K.K. Asogwa, B.S. Goud, N.A. Shah, S. Yook, Rheology of electromagnetohydrodynamic tangent hyperbolic nanofluid over a stretching Riga surface featuring dufour effect and activation energy, Sci. Rep., 12 (2022) 14602.

[21] M. Nadeem, I. Siddique, R. Ali, M.K. Riahi, A.A.A. Mousa, I. Khan, H.M. Hafeez, M. Azam, Dynamics of non-Newtonian tangent hyperbolic liquids conveying tiny particles on objects with variable thickness when Lorentz force and thermal radiation are significant, Front. Phys., 10 (2022) 917677.

[22] S.O. Salawu, M.O. Ogunlaran, E.I. Akinola, O.Y. Oludoun, J.A. Akinpelu, Current density and nonlinear radiation absorber of electromagnetic Williamson thermal migration of F e3O4 and SiO2 nanoparticles in H2O+C2H6O2: A concentrated thermal power, Materials Today Commun., 37 (2023) 107380.

[23] W. Jamshed, K.S. Nisar, R.W. Ibrahim, F. Shahzad, M.R. Eid, Thermal expansion optimization in solar aircraft using tangent hyperbolic hybrid nanofluid: a solar thermal application, J. of Materials Res. and Tech., 14 (2021) 985-1006.

[24] S. Hussain, F. Ahmad, H. Ayed, M.Y. Malik, H. Waqas, M.M. Al-Sawalha, S. Hussain, Combined magnetic and porosity effects on flow of time-dependent tangent hyperbolic fluid with nanoparticles and motile gyrotactic microorganism past a wedge with second-order slip, Case Studies in Thermal Engin., 26 (2021) 100962.

[25] A.R. Hassan, S.O. Salawu, A.B. Disu, O.R. Aderele, Thermodynamic analysis of a tangent hyperbolic hydromagnetic heat generating fluid in quadratic Boussinesq approximation, J. of Comput. Maths. and Data Sci., 4 (2022) 100058.

[26] A. Shafiq, S.A. Lone, T.N. Sindhu, Q.M. Al-Mdallal, G. Rasool, Statistical modeling for bioconvective tangent hyperbolic nanofluid towards stretching surface with zero mass flux condition, Sci. Rep., 11 (2021) 13869.

[27] R.C. Srinivas, B. Mahanthesh, P. Rana, K.S. Nisar, Entropy generation analysis of tangent hyperbolic fluid in quadratic Boussinesq approximation using spectral quasi-linearization method, Appl. Math. Mech. 42(10) (2021) 1524-1542.

[28] A. Aziz, W. Jamshed, T. Aziz, H.M.S. Bahaidarah, K. Ur Rehman, Entropy analysis of Powell-Eyring hybrid nanofluid including effect of linear thermal radiation and viscous dissipation, J. therm. Anal. Calorim., 143(2) (2021) 1331-1343.

[29] S.O. Salawu, A.M. Obalalu, S.S. Okoya, Thermal convection and solar radiation of electromagnetic actuator Cu-Al2O3/C3H8O2 and Cu-C3H8O2 hybrid nanofluids for solar collector optimization, Materials Today Communications, 33(2022) 104763.

[30] S.R. Mishra, S.O. Salawu, R. Baithalu, S. Panda, Multiple slip impact on the micropolar trihybrid nanofluid composed of CNTCu-water over an expanding surface: Spectral weighted residual scheme, Int. J. of Comput. Materials Sci. and Engin., 25 (2025) 500356.

[31] M.A. Qureshi, Thermal capability and entropy optimization for Prandtl-Eyring hybrid nanofluid flow in solar aircraft implementation, Alexandria Engineering J., 61(7) (2022) 5295-5307.

[32] S.O. Salawu, H.A. Ogunseye, E.O. Fatunmbi, MD. Shamshuddin, Energy optimization in zeta potential electroosmotic Casson-Williamson viscous heating magnetized fluid in a convective cooling microchannel, Appl. Thermal Engin., (2025) 128382.

[33] S. Chebaane, S. O. Salawu A.W. Hussein, L. Manai, A. Azhary, K. Manai, A.M. Obalalu, Parametric sensitivities of gravity and electroosmotic-driven ternary composite nanoparticles past a Riga device with heat gain and convective cooling, Int. J. of Modern Physics B, 25 (2025) 2550250.